Chemistry Europe
European Chemical Societies Publishing

WILEY VCH

Excellence in Chemistry Research

Announcing our new flagship journal

- Gold Open Access
- Publishing charges waived
- Preprints welcome
- Edited by active scientists

Meet the Editors of *ChemistryEurope*

Luisa De Cola
Università degli Studi di Milano Statale, Italy

Ive Hermans
University of Wisconsin-Madison, USA

Ken Tanaka
Tokyo Institute of Technology, Japan

ChemPhysChem

Research Article
doi.org/10.1002/cphc.202300647

Chemistry Europe
European Chemical Societies Publishing

www.chemphyschem.org

Indentation Depth-Dependent Hardness of Metal-Organic Framework Crystals: The Effect of Local Amorphization Induced by Indentation

Ximing Chen[+],[a] Bing Wang[+],[a] Penghua Ying,[b] and Jin Zhang*[a]

The hardness of metal-organic frameworks (MOFs) is an important mechanical property metric measuring their resistance to the permanent plastic deformation. The hardness of most MOFs measured from nanoindentation experiments usually exhibits the similar unique indentation depth dependence feature, the mechanism of which still remains unclear. In order to explain the effect of the indentation depth on the hardness of MOFs, we conducted nanoindentation simulations on HKUST-1 by using reactive molecular dynamics simulations. Our simulations reveal that the HKUST-1 material near the indenter can transform from the parent crystalline phase to a new amorphous phase due to the high pressure generated, while its counterpart far from the indenter remains in the crystalline phase. By considering the crystalline-amorphous interface in the energy analysis of MOFs, we derived an analytical expression of the hardness at different indentation depths. It is found that the interface effect can greatly increase the hardness of MOFs, as observed in nanoindentation simulations. Moreover, the proposed analytical expression can well explain the indentation depth-dependent hardness of many MOF crystals measured in nanoindentation experiments. Overall, this work can provide a better understanding of the indentation depth dependence of the hardness of MOFs.

Introduction

Metal-organic frameworks (MOFs) are a fascinating class of nanoporous materials, which are composed of metal clusters and organic linkers. The unique hybrid network topology of MOFs makes the infinite extension of their structures in the three-dimensional space become possible.[1–3] Thus, under the design concept of net chemistry,[3] MOFs can be synthesized by assembling different metal nodes and organic chain ligands together in the similar form of "Lego building", indicating the massive MOF structures for design. In addition, the unique framework structures of MOFs also make their porosity and specific surface area much larger than those of traditional porous materials. For instance, MOF-210 exhibits an extremely large surface area up to 6240 m^2/g, while MOF-200 possesses the highest porosity (up to 90%) ever recorded for crystalline materials.[4] Owing to their superior structural designability and porosity characteristics, MOFs have shown broad application prospects in many fields.[5–9]

Most of currently synthesized MOFs are small-sized particulate polycrystals, which are thus needed to be further densified by powder engineering to obtain a large-sized solid MOF structure. During the densification process of open framework materials (OFMs) including MOFs and their organic analogues, covalent organic frameworks (COFs), for industrial applications, they are usually subjected pressures with several hundred megapascals. Such large pressure may cause large deformations and eventually the mechanical instability of OFMs.[10–16] Thus, understanding the mechanical behaviours and properties of MOFs is essential for their technical applications. Among various mechanical property metrics, the hardness of MOFs is an important parameter measuring their resistance to the permanent plastic deformation. The nanoindentation test either based on the instrumented nanoindenter or atomic force microscopy is the most widely used technique to experimentally measure the hardness of MOFs.[10–12] To date, the nanoindentation has been employed to extract the hardness of many representative MOF materials, such as HKUST-1, ZIF-8 and MOF-5.[17–21] It is shown that ZIF-8 and HKUST-1 possess the comparable hardness, which is much larger than that of MOF-5. Nevertheless, the hardness of all MOFs is found to be generally lower than that of their pure inorganic counterparts, which indicates that additional caution is required in the postprocessing fabrication of MOFs.[12] In addition, a unique depth dependency of hardness is similarly observed in almost all nanoindentation tests of MOFs, in which the hardness of almost all tested MOFs decreases as the indentation depth grows and, ultimately, tends to a convergence after a certain indentation depth.[17–21] To date, the mechanism of the depth-dependent hardness observed in MOFs is still unclear, which thus deserves a comprehensive study.

As mentioned above, the hardness of MOFs is usually measured through nanoindentation tests. In this work, by

[a] X. Chen,[+] B. Wang,[+] Prof. Dr. J. Zhang
School of Science, Harbin Institute of Technology, 518055 Shenzhen, PR China
E-mail: jinzhang@hit.edu.cn
Homepage: https://lamb.mysxl.cn

[b] Dr. P. Ying
Department of Physical Chemistry, School of Chemistry, Tel Aviv University, 6997801 Tel Aviv, Israel

[+] Contributed equally

Supporting information for this article is available on the WWW under https://doi.org/10.1002/cphc.202300647

taking HKUST-1 as a typical example, indentation responses of MOFs are studied by reactive molecular dynamics (MD) simulations. The atomic displacement of HKUST-1 materials under indentation is examined. A crystalline-to-amorphous phase transition is found to occur in the HKUST-1 material near the indenter, which is also confirmed by the simulations under hydrostatic pressure. Inspired by observations of MD simulations, an analytical expression describing the hardness at different indentation depths is derived, which can well explain the indentation depth dependence of hardness of many MOF crystals measured in nanoindentation experiments.

Methods

Nanoindentation simulations. The HKUST-1 material considered here contains metal centres of Cu atoms and organic linkers of C, H and O atoms. As a representative example, the [100]-oriented HKUST-1 crystal was constructed for nanoindentation simulations, which was considered in the previous experiments.[21] The HKUST-1 sample considered here has the size of 158 Å×158 Å×158 Å. As shown in Figure 1a, to conduct the nanoindentation simulations, the HKUST-1 models were divided into three regions that are the Newtonian, thermostat, and frozen regions. Specifically, atoms in the Newtonian region following the Newtonian dynamics were used to simulate the nanoindentation. The thermostat region with a thickness of 10 Å was used to simulate the heat dissipation process and stabilize the temperature of models. Atoms in the frozen region with a thickness of 5 Å were fixed to support the whole HKUST-1 models. The thermostat and frozen regions with the similar thicknesses were widely employed in the previous nanoindentation simulations.[22,23] The ReaxFF potential with potential parameters taken from Ref. [24] was employed to describe the interactions between atoms in HKUST-1, since it has the capacity to accurately simulate the mechanical responses of HKUST-1.[25,26] A virtual spherical indenter having a radius of 30 Å was used here,

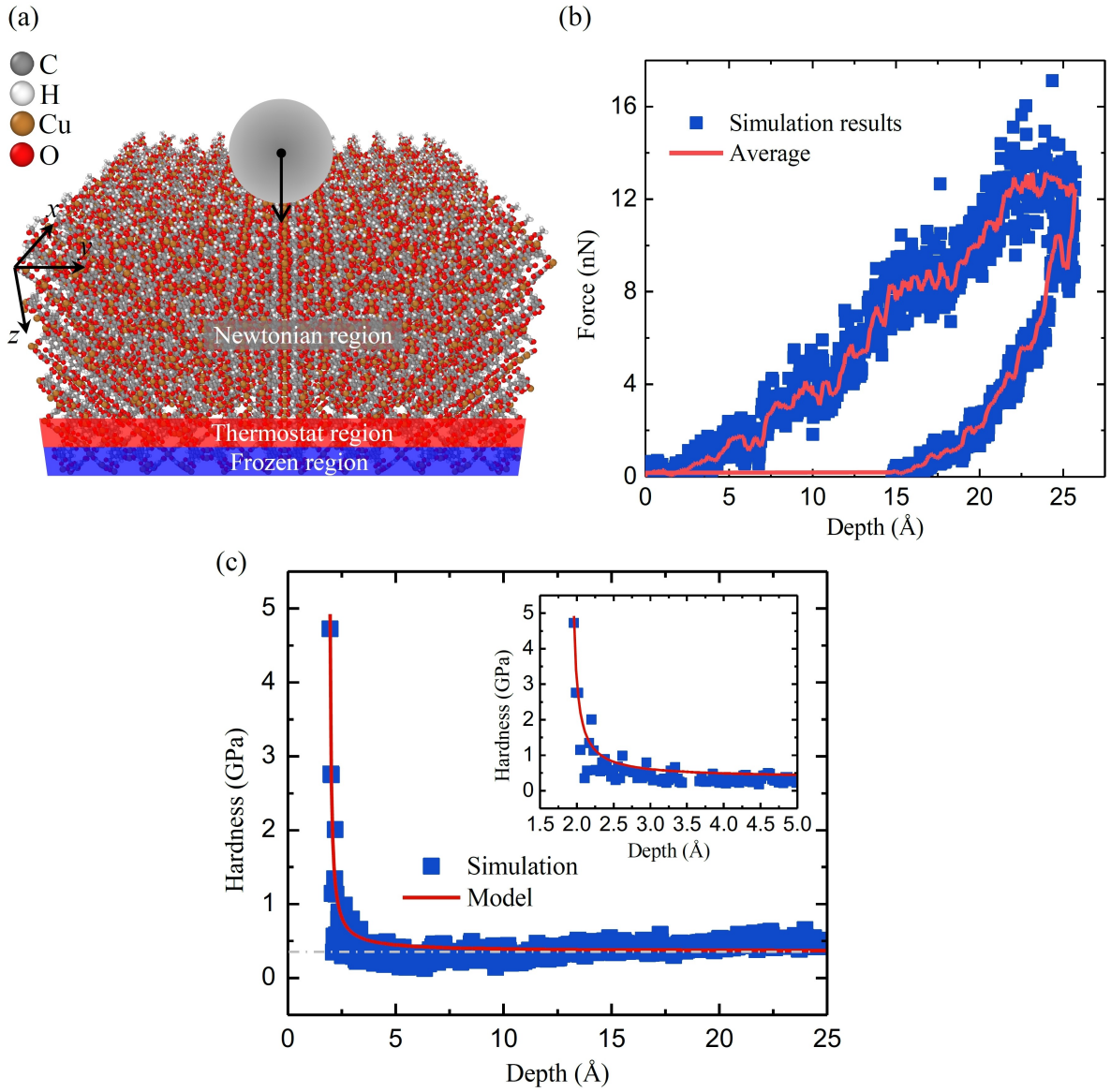

Figure 1. (a) Schematic of the nanoindentation simulations of [100]-oriented HKUST-1 crystals. (b) Indentation force-depth curve of the HKUST-1 material extracted from MD simulations. (c) Evolution of the hardness with growing indentation depth.

which can generate a repulsive force on each atom in the indented HKUST-1 given as $F(r)=K(r-R)^2$, where $K=10$ eV/Å^3 is the force constant, r is the distance from the atom to the indenter centre, and R is the radius of the indenter. As shown in Figure S1, the radius of 30 Å selected here has the capacity to obtain a stable hardness. Non-zero values of the repulsive force can be extracted only when $r<R$. Before each nanoindentation simulation, the conjugate gradient algorithm was performed to relax the HKUST-1 model to a minimum energy state, which was followed by an NVT simulation with 4 ps to minimize the internal energy and make the model reach an equilibrium state. During the nanoindentation process, the indenter initially 4 Å above the HKUST-1 surface was gradually pushed into the sample and then pulled out from it with the same velocity of 3 Å/ps, since no significant change was observed in the force-depth results if keeping decreasing the indentation velocity (see Figure S2 in the Supporting Information). In the simulations, the NVE ensemble was applied to the Newtonian region, while the NVT ensemble with Langevin thermostat was used for the thermostat region. All simulations performed at room temperature (300 K) were implemented by using open-source code LAMMPS.[27] Periodic boundary conditions applied in the transverse directions, while the top free [100] surface was assumed to be terminated by acetate groups (see Figure S3 in the Supporting Information).[28]

Simulations under hydrostatic pressure. A 3×3×3 HKUST-1 supercell with the [100] orientation was considered in simulations. Periodic boundaries were applied in all directions. Here, the HKUST-1 materials were similarly described by the ReaxFF potential. Before the simulations under hydrostatic pressure were conducted, the structural relaxations similarly as described above were conducted to achieve the equilibrium structures of HKUST-1 models. During the compression process, the pressure was increased from 0 to 500 MPa within 500 ps, which was completely unloaded to 0 MPa with the same rate. Here, the NsT ensemble was employed to realize the simulations under hydrostatic pressure, while the Nosé-Hoover thermostat was used to control the pressure and constrain the system temperature at the room temperature. Input files of MD simulations conducted in the present study are available in the data repository through https://github.com/bing93wang/MOF-hardness.

Results and Discussion

When a [100]-oriented HKUST-1 model was indented with a maximum indentation depth of 25 Å as shown in Figure 1a, the corresponding force-depth curve during the whole nanoindentation process is shown in Figure 1b. Here, the force acting on the indenter equals to the sum of resultant forces of surrounding atoms on the *z*-direction. In general, the force continuously increases as the indentation depth continues to increase until it reaches a maximum depth. After reaching the maximum depth, although the indenter returns to its original position to completely release the force, a large irrecoverable deformation with a magnitude of 15 Å is still retained in HKUST-1, indicating the significant plasticity of HKUST-1. To better illustrate the plastic deformation generated by nanoindentations, in Figure 2a we show typical snapshots of atomic displacement of HKUST-1 materials during the loading process. As expected, the atomic displacement of the indentation area becomes larger as the indentation depth increases. Moreover, the deformation of HKUST-1 under indentation is also found to be majorly induced by the densification of materials near the indenter. In Figure 2b, we show the evolution of the percentage of Cu–O coordination numbers (discrete values of 2, 3, and 4) of the region near the indenter during whole indentation process. It is found that the 4-fold coordination decreases from 1 to 0.7 as the indentation depth grows from 0 Å to 25 Å in the loading process. In the same loading process, the 3-fold coordination correspondingly increases from 0 to 0.30. The change in the percentage of Cu–O coordination numbers during the loading process indicates that the densification of HKUST-1 material near the indenter is accompanied with the destruction of some Cu–O coordination bonds. Moreover, the destruction of Cu–O coordination is irrecoverable, since 3- and 4-fold coordination numbers keep almost unchanged at 0.19 and 0.79, respectively, during the unloading process, which, to some extent, indicates the thermodynamical stability of the deformed structure of HKUST-1 under indentation. Moreover, the above findings also illustrate that the significant plasticity of HKUST-1 under indentation is ascribed to the destruction of the Cu–O coordination bonds in the densification process of HKUST-1 near the indenter.

To quantitatively measure the capability of the HKUST-1 models considered in the present nanoindentation simulations to resist the permanent plastic deformation, we calculated their hardness H by dividing the indentation force F by the surface contact area A_c, i.e.,

$$H=\frac{F}{A_c}. \tag{1}$$

Here, the contact area was approximated as $A_c=\pi h(2R-h)$,[22,23,29] where h is the indentation depth.

According to Equation 1, the hardness of HKUST-1 predicted from the present simulations depends on the indentation depth, as shown in Figure 2c. Specifically, when the indentation depth is smaller than ~4 Å, the hardness significantly decreases as the indentation depth grows. The significant decrease of the hardness of HKUST-1 with growing indentation depth was also observed in recent indentation experiments,[19,21] the explanation of which will be discussed latter. When the indentation depth becomes than ~4 Å, the hardness tends to be stable and converges to a value of ~384 MPa, which is close to the converged hardness values of 410 MPa and 460 ± 30 MPa measured from two recent nanoindentation experiments.[19,21]

It is known that the during the indentation process, a high pressure will be generated near the indenter. To mimic the mechanical responses of the highly-pressured HKUST-1 near the indenter, we conducted the simulations for HKUST-1 under hydrostatic pressure. In Figure 3a, we show the volume strain of HKUST-1 in response to different hydrostatic pressures. Here, the volume strain was defined as $\varepsilon=(V-V_0)/V_0$ with V and V_0, respectively, being the volume of the compressed HKUST-1 and the initial volume of HKUST-1 without compression. Initially, the volume strain linearly grows as the pressure grows, indicating the elastic deformation of HKUST-1 in this process. However, when the pressure reaches around 321 MPa, the volume strain dramatically increases from 0.05 to 0.45, which indicates the

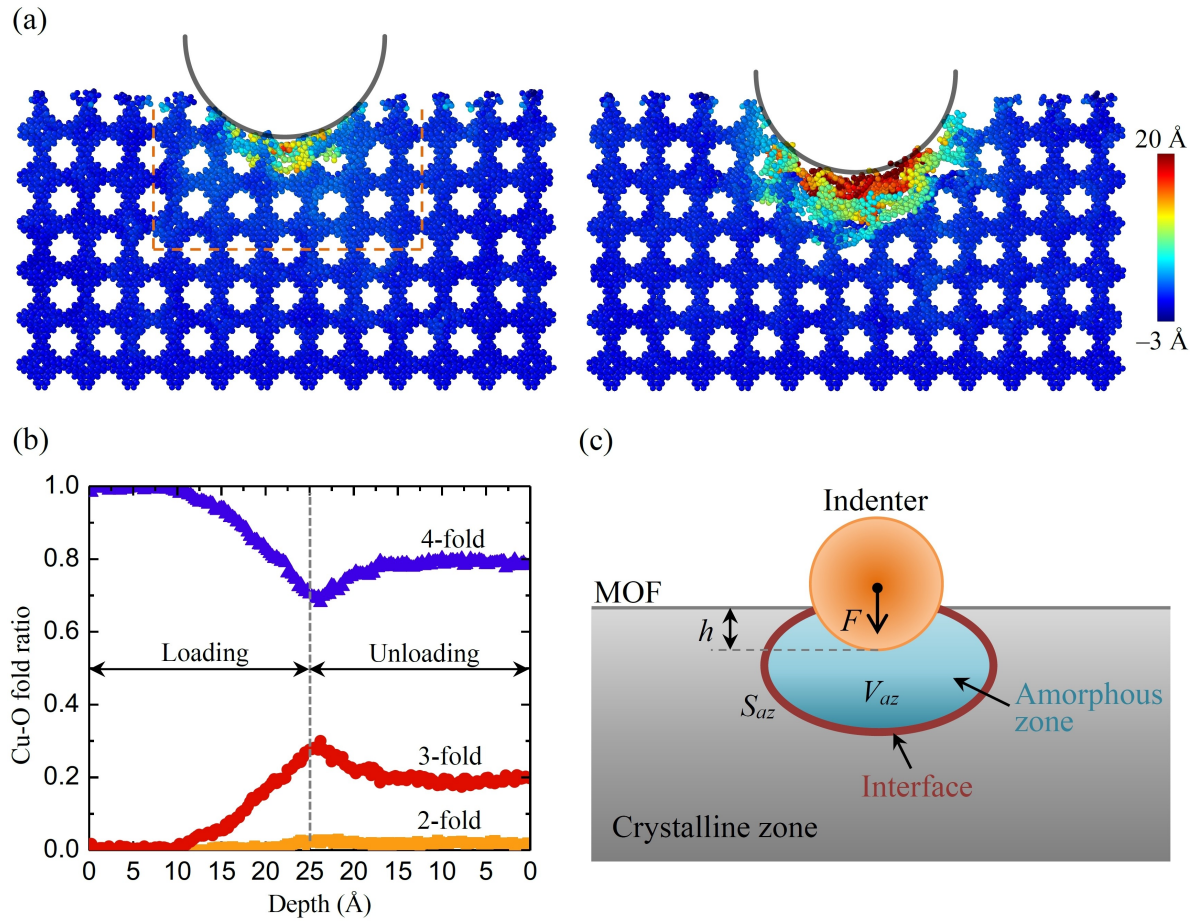

Figure 2. (a) Atomic displacements of HKUST-1 at indentation depths of 15 Å (left) and 25 Å (right). Here, atoms are coloured according to their displacements in the indentation direction. (b) Evolution of the percentage of Cu–O coordination numbers of HKUST-1 near the indenter as noted by the rectangle in (a) during the whole indentation process. (c) Schematic depiction of the coexistence of the parent crystalline phase and the transformed amorphous phase in the HKUST-1 material under indentation.

occurrence of the structural collapse of HKUST-1. Actually, a similar sudden volume drop was also observed in very recent *in situ* compression experiments of HKUST-1 micropillars when they are under the compressive load around 300 MPa.[29,30] The structural collapse results in the transformation of HKUST-1 from the parent crystalline phase to a new amorphous phase as shown in Figure 3b. The different structure characteristics between crystalline and amorphous phases also can be verified by the difference of their radial distribution functions (RDFs) as shown in Figure 3c, which are widely used to characterise the overall molecular structures. To further verify the amorphization of HKUST-1 predicted from ReaxFF simulations, in Figure S4 we show RDFs of the compressed HKUST-1 with volume strains of 2% and 43%, calculated from the structures relaxed by density functional theory (DFT) calculations. It is found that RDFs of crystalline HKUST-1 with a small strain of 2% show long-range correlations exhibiting a pattern with discontinuous and sharp peaks along the given range. However, RDFs of the structure with a large strain of 43% contain relatively less intense peaks up to 3 Å, which thus present typical characteristics of an amorphous state such that it has a well-defined short-range order and the lack of long-range correlations. This finding can serve as a piece of evidence proving the pressure-induced amorphization of HKUST-1 observed in ReaxFF simulations. After the completeness of the phase transition of HKUST-1 or when the volume strain is larger than 0.45, the volume strain is found to increase linearly with increasing pressure again, which indicates the elastic deformation of HKUST-1 within the amorphous phase. Moreover, as shown in Figure 3a, the amorphous phase of HKUST-1 due to the structural collapse will not recover to its original crystalline phase even after the complete release of pressure. Theoretically, an idealized model shown in the inset of Figure 3a can be used to simply describe the phase transition of HKUST-1 under compression. The pressure-induced phase transition of HKUST-1 was observed in many existing experiments,[31,32] though the critical pressure of phase transition detected in experiments is much higher than the value obtained here, which is probably ascribed to the effect of guest adsorption in experiments.[33] The similar crystalline-to-amorphous phase transition induced by compression was also observed in many other MOF materials such as ZIF-8,[34–36] MOF-5,[37] and isoreticular DUT materials.[38,39] Moreover, as illustrated in the Supporting Information (Figure S5), the change in the percentage of Cu–O coordination numbers

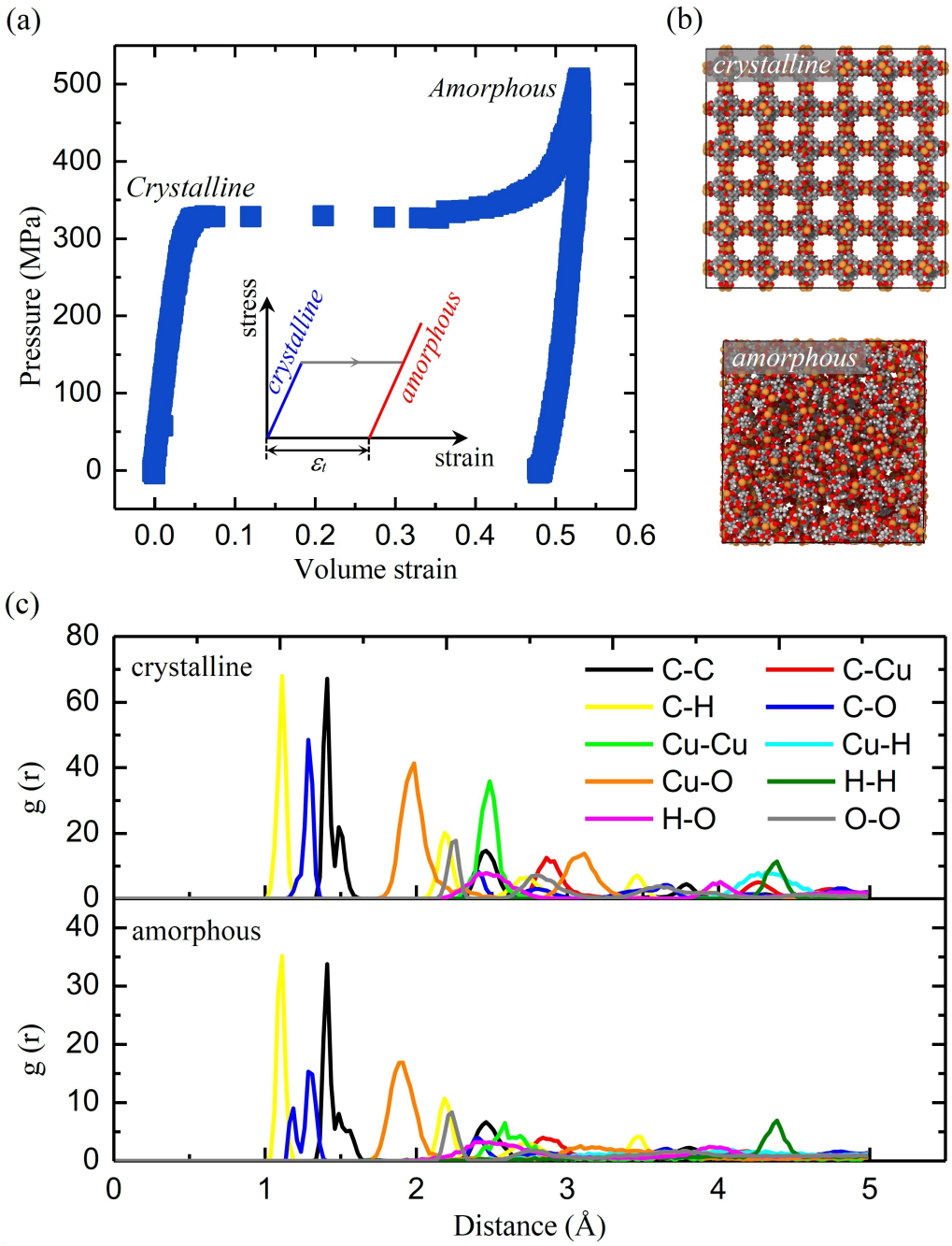

Figure 3. (a) Evolution of the volume strain during the loading and unloading processes of the HKUST-1 crystal under hydrostatic pressure. The inset shows an idealized model illustrating the crystalline-to-amorphous phase transitions of HKUST-1 under pressure. (b) Atomic structures of the parent crystalline phase and the transformed amorphous phase of HKUST-1. (c) RDFs $g(r)$ of crystalline and amorphous phases of HKUST-1.

after the phase transition obtained now is qualitatively close to that of the HKUST-1 material under indentation loading (Figure 2b), which, to some extent, indicates that the deformed HKUST-1 under the indenter may exhibit a structure topologically similar to the amorphous phase induced by pressure. It is also noted here that the HKUST-1 crystals considered in the present simulations were assumed to have a perfect structure, while HKUST-1 crystals synthesised in experiments may naturally possess defects.[40,41] Nevertheless, according to our recent study,[26] the pressure-induced crystalline-to-amorphous phase transition may similarly occur in HKUST-1 materials with missing linker defects in spite of a smaller critical pressure of phase transition was observed in the defective HKUST-1.

From the above discussion, we can see that the high pressure under the indenter can render the HKUST-1 material nearby transfer from the crystalline phase to the amorphous phase. In other words, there exist both the amorphous and crystalline phases in the HKUST-1 under indentation, which, respectively, locate at the regions near and far from the indenter. Indeed, as shown in Figure S6, RDFs of the HKUST-1

material near the indenter exhibit the well-defined short-range order and the lack of long-range correlations even after completely unloading, which indicates the irreversible transition of the crystalline phase to the amorphous phase of HKUST-1 due to indentation. Moreover, RDFs of the HKUST-1 material near the indenter after unloading are also found to be similar to those of amorphous HKUST-1 predicted from DFT calculations (see Figure S7), which further indicates the applicability of the present ReaxFF potential in simulating the crystalline-to-amorphous phase transition of HKUST-1 during the indentation process. It is also noted here that although the present ReaxFF potential can majorly capture the crystalline-to-amorphous phase transition of HKUST-1 due to indentation, precisely identifying the mechanical properties of amorphous HKUST-1 based on the present ReaxFF potential is still a challenge,[42] because it was not specifically parameterized for the amorphous HKUST-1.[24] Nevertheless, this quantitative discrepancy trivially affects the present study because the major aim of the nanoindentation simulations conducted here is to provide atomistic insights into the deformation mechanism of HKUST-1 under indentation rather than quantitatively measure the mechanical properties of HKUST-1. Indeed, the parameterization of force fields specifically for amorphous HKUST-1 deserves a comprehensive study in the near future. Due to the coexistence of crystalline and amorphous phases in the HKUST-1 materials, there should exist an interface between crystalline and amorphous phases of HKUST-1 as shown in Figure 2c. Therefore, the variation of the total free energy of the HKUST-1 system under indentation is comprised of the mechanical energy of external force U_e, the interface energy U_i, the bulk elastic strain energy U_{be}, and the bulk chemical free energy U_{bc}. In other words, the total Gibbs free energy G of the HKUST-1 system under indentation can be expressed as:[43]

$$G = U_e + U_i + U_{be} + U_{bc}. \tag{2}$$

In Equation 2, $U_e = -Fh$, where F is the indentation force. The similar free energy was also assumed in the previous theoretical study of nanoindentation of shape memory alloys,[44] which similarly exhibit the phase coexistence during the indentation process. As shown in Figure 2a, the deformation of the HKUST-1 system under the indenter majorly occurs in its transformed amorphous zone. Thus, U_{be} and U_{bc} in Equation 2 are determined by the volume V_{az} of the transformed amorphous zone, while U_i should be determined by the surface area S_{az} of the amorphous zone. In other words, U_{be}, U_{bc} and U_i can be written as follows:

$$U_{be} = \frac{1}{2}\int_{V_{az}} E[\varepsilon(x,y,z)]^2 dv,\ U_{bc} = \int_{V_{az}} \Delta G(T,x,y,z) dv,\\ U_i = \frac{1}{2}\int_{S_{az}} klE_1[\varepsilon(x,y,z)]^2 ds, \tag{3}$$

where E is the Young's modulus of HKUST-1, ε is the strain, ΔG is the change in chemical free energy density with T being the temperature, E_1 is the equivalent interfacial elastic modulus, k is a small-scale coefficient and l is the characteristic thickness of interface. Because the only length parameter in the present system is the indentation depth h, the integral of U_{be} and U_{bc} in Equation 3 thus should be proportional to h^3, while the integral of U_i should be proportional to h^2. These relationships also can be verified by the fact that the number of the atoms in the amorphous zone is approximately proportional to the cube of the indentation depth, as shown in Figure S8. After introducing the non-dimensional shape factors α_1, α_2 and α_3, Equation 3 can be further rewritten as:

$$U_{be} = \alpha_1 E\varepsilon_t^2 h^3,\ U_{bc} = \alpha_2 \Delta G(T) h^3,\ U_i = \alpha_3 klE_1\varepsilon_t^2 h^2, \tag{4}$$

where ε_t is the characteristic transformation strain as illustrated in the inset of Figure 3a.

Using the energy minimization principal, the equilibrium condition of the HKUST-1 system needs to satisfy the following equation:

$$\frac{\partial G}{\partial h} = 0. \tag{5}$$

After substituting Equations 2 and 4 into Equation 5, we obtain the following expression for the indentation force F:

$$F = 2\alpha_3 klE_1\varepsilon_t^2 h + 3\alpha_1 E\varepsilon_t^2 h^2 + 3\alpha_2 \Delta G h^2, \tag{6}$$

Further substituting Equation 6 into Equation 1 and considering the contact area $A_c = \beta h^2$ (β is a non-dimensional parameter depending on the geometry of the indenter tip), the hardness H can be expressed as follows:

$$H(h) = H_\infty + \gamma\left(\frac{l}{h}\right), \tag{7}$$

where $H_\infty = \dfrac{3\alpha_1 E\varepsilon_t^2 + 3\alpha_2 \Delta G}{\beta}$ and $\gamma = \dfrac{2\alpha_3 kE_1\varepsilon_t^2}{\beta}$.

The hardness expressed by Equation 7 is found to be dependent on the indentation depth h. Moreover, the indentation depth dependence of hardness is ascribed to the interface effect that is measured by the ratio of l/h. Specifically, when the indentation depth h is comparable to the characteristic thickness of interface l, the interface effect becomes significant, resulting in a detectable indentation depth dependence of the indentation hardness. When the indentation depth is large enough at $l/h \to 0$, the interface effect becomes ignorable. Under this circumstance, H converges to H_∞, which represents a hardness of MOFs at the infinite depth. Thus, Equation 7 can be simply adopted to predict the intrinsic hardness of MOFs absence of the influence of finite indentation depth.

To further validate the theoretical model (Equation 7) proposed here, in Figure 4 we show experimentally measured hardness values of some representative MOFs (HKUST-1, ZIF-8 and MOF-5) at different indentation depths. It is noted that only the hardness values at depths larger than 100 nm were considered here, because in nanoindentation tests perturba-

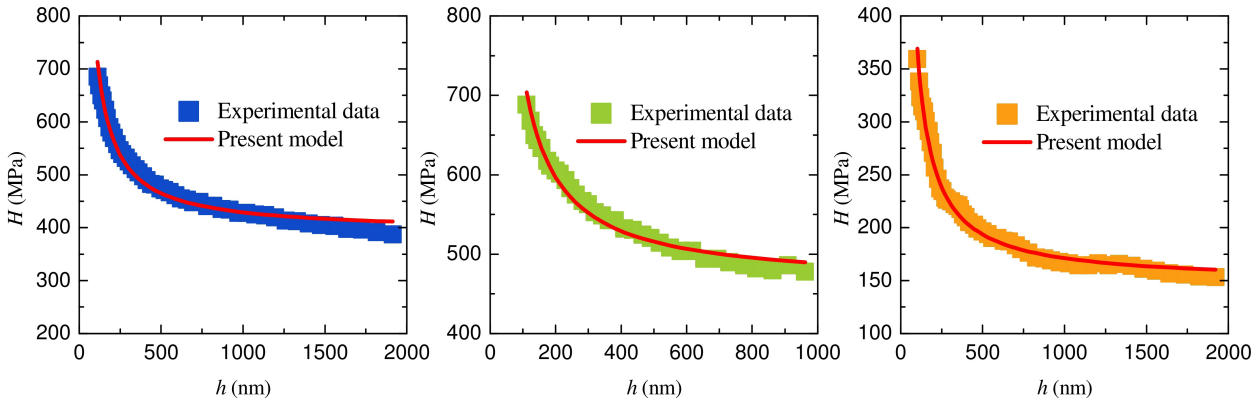

Figure 4. The size dependence of the hardness of HKUST-1, ZIF-8 and MOF-5 extracted from nanoindentation experiments,[17–19] which can be well fitted by the present theoretical model (Equation 7).

tions due to some extrinsic factors such as surface roughness, tip radius and thermal drift may become significant when the indentation depth is relatively small. In general, it is found that the indentation depth-dependent hardness of HKUST-1, ZIF-8 and MOF-5 observed in nanoindentation experiments can be well captured by the present theoretical model (Equation 7).[17–19] Intrinsic hardness values of HKUST-1, ZIF-8 and MOF-5 predicted from Equation 7 are 392 MPa, 461 MPa and 149 MPa, respectively. Moreover, the indentation depth-dependent hardness of HKUST-1 obtained from MD-based nanoindentation simulations can be similarly fitted by the present model (see Figure 3c). It is worth noting here that all the calculation and theoretical analyses of hardness were based on the existing experimental date of the measured load-depth curves of MOFs. It is thus desirable to make some more experimental efforts to verify the proposed theoretical model in the future. In addition, a direct calculation of the characteristic length scale of interface via the experiments or simulations is still deserves a comprehensive study.

Conclusions

In summary, the nanoindentations of HKUST-1 were simulated by ReaxFF MD simulations. Our MD simulations illustrate that the high pressure under the indenter can trigger the crystalline-to-amorphous phase transition of HKUST-1 near the indenter, making it transform from the parent crystalline phase to a new amorphous phase. As a result, both crystalline and amorphous phases coexist in the HKUST-1 material under indentation. After introducing the contribution of the crystalline-amorphous interface in the energy analysis, we derived an analytical expression of the hardness at different indentation depths, which can well explain the indentation depth dependence of hardness of many MOF materials measured in nanoindentation experiments. Our theoretical model also reveals that the indentation depth dependence of hardness is ascribed to the competition between the bulk and interface deformations during the crystalline-to-amorphous phase transition process. Overall, the present study not only enhances our understanding of the indentation depth dependence of hardness of MOFs, but also provides a theoretical avenue to extract the intrinsic hardness of MOFs by excluding the effect of the finite indentation depth.

Acknowledgements

This work was supported by the Guangdong Basic and Applied Basic Research Foundation (Grant No. 2022A1515010631) and Shenzhen Science and Technology Program (Grant No. GXWD20220811164345003).

Conflict of Interests

The authors declare no conflict of interest.

Data Availability Statement

The data that support the findings of this study are available from the corresponding author upon reasonable request.

Keywords: metal-organic frameworks · hardness · indentation depth dependence · phase transition · high-pressure

[1] J. T. Li, P. M. Bhatt, J. Y. Li, M. Eddaoudi, Y. L. Liu, *Adv. Mater.* **2020**, *32*, 2002563.
[2] S. Dou, X. G. Li, X. Wang, *ACS Materials Lett.* **2020**, *2*, 1251–1267.
[3] O. M. Yaghi, M. O'Keeffe, N. W. Ockwig, H. K. Chae, M. Eddaoudi, J. Kim, *Nature* **2003**, *423*, 705–714.
[4] H. Furukawa, N. Ko, Y. B. Go, N. Aratani, S. B. Choi, E. Choi, A. Ö. Yazaydin, R. Q. Snurr, M. O'Keeffe, J. Kim, O. M. Yaghi, *Science* **2010**, *329*, 424–428.
[5] A. Schneemann, V. Bon, I. Schwedler, I. Senkovska, S. Kaskel, R. A. Fischer, *Chem. Soc. Rev.* **2014**, *43*, 6062–6096.
[6] L. Wang, Y. Z. Han, X. Feng, J. W. Zhou, P. F. Qi, B. Wang, *Coord. Chem. Rev.* **2016**, *307*, 361–381.
[7] H. B. Wu, X. W. Lou, *Sci. Adv.* **2017**, *3*, eaap9252.
[8] X. Zhou, Y. R. Miao, K. S. Suslick, D. D. Dlott, *Acc. Chem. Res.* **2020**, *53*, 2806–2815.
[9] N. Hanikel, M. S. Prévot, O. M. Yaghi, *Nat. Nanotechnol.* **2020**, *15*, 348–355.

[10] N. C. Burtch, J. Heinen, T. D. Bennett, D. Dubbeldam, M. D. Allendorf, *Adv. Mater.* **2017**, *30*, 1704124.
[11] L. R. Redfern, O. K. Farha, *Chem. Sci.* **2019**, *10*, 10666–10679.
[12] J. C. Tan, A. K. Cheetham, *Chem. Soc. Rev.* **2011**, *40*, 1059–1080.
[13] J. Zhang, *Phys. Chem. Chem. Phys.* **2018**, *20*, 29462–29471.
[14] J. Sun, A. Iakunkov, I. A. Baburin, B. Joseph, V. Palermo, A. V. Talyzin, *Angew. Chem. Int. Ed.* **2020**, *59*, 1087–1092.
[15] H. Y. Li, J.-L. Brédas, *Chem. Mater.* **2021**, *33*, 4529–4540.
[16] M. Erkartal, *Comput. Mater. Sci.* **2023**, *227*, 112275.
[17] J. C. Tan, T. D. Bennett, A. K. Cheetham, *Proc. Natl. Acad. Sci. USA* **2010**, *107*, 9938–9943.
[18] J. Y. Jung, F. Karadas, S. Zulfiqar, E. Deniz, S. Aparicio, M. Atilhan, C. T. Yavuz, S. M. Han, *Phys. Chem. Chem. Phys.* **2013**, *15*, 14319–14327.
[19] T. Tian, Z. X. Zeng, D. Vulpe, M. E. Casco, G. Divitini, P. A. Midgley, J. Silvestre-Albero, J.-C. Tan, P. Z. Moghadam, D. Fairen-Jimenez, *Nat. Mater.* **2018**, *17*, 174–179.
[20] Z. X. Zeng, J.-C. Tan, *ACS Appl. Mater. Interfaces* **2017**, *9*, 39839–39854.
[21] J. Heinen, A. D. Ready, T. D. Bennett, D. Dubbeldam, R. W. Friddle, N. C. Burtch, *ACS Appl. Mater. Interfaces* **2018**, *10*, 21079–21083.
[22] H.-T. Luu, S.-L. Dang, T.-V. Hoang, N. Gunkelmann, *Appl. Surf. Sci.* **2021**, *551*, 149221.
[23] J. L. Zhou, Z. J. Jiao, J. Zhang, Z. Zhong, *J. Alloys Compd.* **2021**, *878*, 160336.
[24] S. Monti, C. Li, V. Carravetta, *J. Phys. Chem. C* **2013**, *117*, 5221–5228.
[25] S. A. Mohamed, J. Kim, *J. Phys. Chem. C* **2021**, *125*, 4509–4518.
[26] B. Wang, P. H. Ying, J. Zhang, *J. Phys. Chem. C* **2023**, *127*, 2533–2543.
[27] A. P. Thompson, H. M. Aktulga, R. Berger, D. S. Bolintineanu, W. M. Brown, P. S. Crozier, P. J. in't Veld, A. Kohlmeyer, S. G. Moore, T. D. Nguyen, R. Shan, M. J. Stevens, J. Tranchida, C. Trott, S. J. Plimpton, *Comput. Phys. Commun.* **2022**, *271*, 108171.
[28] S. Amirjalayer, M. Tafipolsky, R. Schmid, *J. Phys. Chem. Lett.* **2014**, *5*, 3206–3210.
[29] A. J. Bushby, N. M. Jennett, *Mater. Res. Soc. Symp. Proc.* **2001**, *649*, Q7.17.
[30] Z. X. Zeng, Y. Xiao, J. M. Wheeler, J.-C. Tan, *Commun. Chem.* **2023**, *6*, 63.
[31] K. W. Chapman, G. J. Halder, P. J. Chupas, *J. Am. Chem. Soc.* **2008**, *130*, 10524–10526.
[32] A. J. Graham, J.-C. Tan, D. R. Allan, S. A. Moggach, *Chem. Commun.* **2012**, *48*, 1535–1537.
[33] L. Vanduyfhuys, S. M. J. Rogge, J. Wieme, S. Vandenbrande, G. Maurin, M. Waroquier, V. Van Speybroeck, *Nat. Commun.* **2018**, *9*, 204.
[34] P. H. Ying, J. Zhang, X. Zhang, Z. Zhong, *J. Phys. Chem. C* **2020**, *124*, 6274–6283.
[35] A. U. Ortiz, A. Boutin, A. H. Fuchs, F.-X. Coudert, *J. Phys. Chem. Lett.* **2013**, *4*, 1861–865.
[36] M. Erkartal, M. Durandurdu, *Mater. Chem. Phys.* **2020**, *240*, 122222.
[37] M. Erkartal, M. Durandurdu, *ChemistrySelect* **2018**, *3*, 8056–8063.
[38] P. H. Ying, J. Zhang, Z. Zhong, *Microporous Mesoporous Mater.* **2021**, *312*, 110765.
[39] P. H. Ying, J. Zhang, Z. Zhong, *J. Phys. Chem. C* **2021**, *125*, 12991–13001.
[40] F. S. Gentile, M. Pannico, M. Causà, G. Mensitieri, G. Di Palma, G. Scherillo, P. Musto, *J. Mater. Chem. A* **2020**, *8*, 10796–10812.
[41] T. Wang, H. Zhu, Q. Zeng, D. Liu, *Adv. Mater. Interfaces* **2019**, *6*, 1900423.
[42] N. Castel, F.-X. Coudert, *J. Phys. Chem. C* **2022**, *126*, 19532–19541.
[43] R. Hill, in *The Mathematical Theory of Plasticity*, Oxford University Press, New York, **1950**.
[44] W. Y. Yan, A. Amini, Q. P. Sun, *J. Mater. Res.* **2013**, *28*, 2031–2039.

Manuscript received: September 9, 2023
Revised manuscript received: October 13, 2023
Accepted manuscript online: October 15, 2023
Version of record online: ■■, ■■

RESEARCH ARTICLE

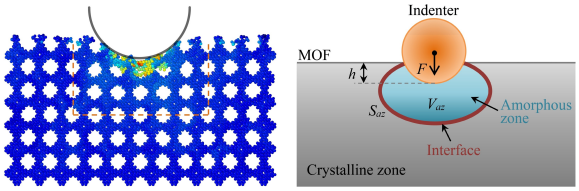

*X. Chen, B. Wang, Dr. P. Ying, Prof. Dr. J. Zhang**

1 – 9

Indentation Depth-Dependent Hardness of Metal-Organic Framework Crystals: The Effect of Local Amorphization Induced by Indentation

Based on reactive molecular dynamics simulations, a local crystalline-to-amorphous phase transition occurring in HKUST-1 crystals under indentation is reported. By considering the effect of two-phase interface, an analytical expression of hardness is derived that explains the size dependence of hardness of many metal-organic framework crystals measured in experiments.